Electronic Supplementary Material (ESI) for Nanoscale.

*– Supplementary Information –*

# Carbon Nanofiber High Frequency Nanomechanical Resonators

Jaesung Lee[1], Anupama B. Kaul[2], Philip X.-L. Feng[1,*]

[1]*Department of Electrical Engineering & Computer Science, Case School of Engineering,*
*Case Western Reserve University, Cleveland, OH 44106, USA*
[2]*Department of Electrical and Computer Engineering*
*The University of Texas at El Paso, El Paso, TX 79968, U.S.A.*

## Table of Contents

---

[*] Corresponding Author. Email: philip.feng@case.edu

## S1. CNF Resonator with High *Q*

Here we show an example of a carbon nanofiber (CNF) resonator with slightly higher *Q*uality (*Q*) factor. Figure S1 shows the measured thermomechanical motion, and for this device, we find the resonance frequency of $f \approx 5.945$MHz with the $Q$ of 760, achieving figure of merit of $f \times Q = 4.5 \times 10^9$Hz.

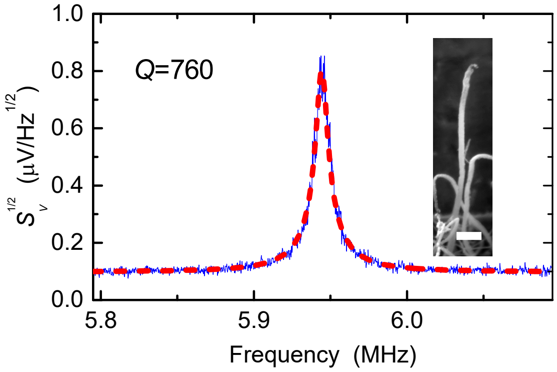

**Figure S1**. Measured thermomechanical motion of the CNF with $f \approx 5.945$MHz and $Q \approx 760$. Scale bar is 300nm.

## S2. Cantilever with Pinned-Free Boundary Condition

In this section, we show detailed multimode resonance behaviors of CNF cantilevers. Flexural resonance motions of the cantilever with pinned-free boundary conditions ($Z_n(0)=d^2Z_n(0)/dx^2=0$, and $d^2Z_n(1)/dx^2=d^3Z_n(1)/dx^3=0$) are given by

$$Z_n(x) = \left(\sin\left(\beta_n x\right) - \sinh\left(\beta_n x\right)\right) + \frac{\left(\beta_n^2 \sin\left(\beta_n\right) + \beta_n^2 \sinh\left(\beta_n\right)\right)}{\left(-\beta_n^2 \sin\left(\beta_n\right) + \beta_n^2 \sinh\left(\beta_n\right)\right)}\left(\sin\left(\beta_n x\right) + \sinh\left(\beta_n x\right)\right), \quad \text{(S1)}$$

where, $\beta_n$ is the mode dependent parameters (*e.g.*, $\beta_1$=3.927, $\beta_2$=7.069, and $\beta_3$=10.210), $x$ is the normalized cantilever position by length ($0 \leq x \leq 1$). Using Eq. S1, we plot resonance motions of the 1st, 2nd, and 3rd modes (Fig. 2(a-c)) from the CNF. We note that the fundamental resonance mode shape of a conventional clamped-free cantilever does not exist in the one with the pinned-free boundary conditions (because it transforms to rigid body rotation ($\beta_0$=0 thus $f$=0Hz)).

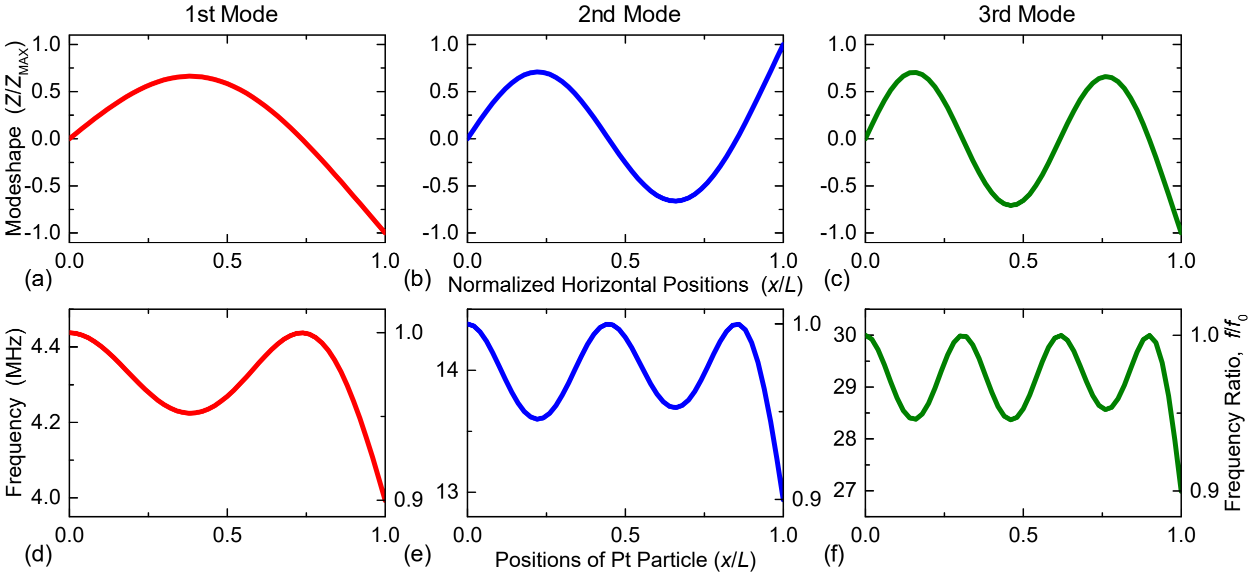

**Figure S2**. Calculated resonance mode shapes of a CNF cantilever with pinned-free boundary conditions. (a-c) 1st, 2nd, and 3rd resonance mode shapes. (d-f) Calculated resonance frequency of the CNF ($L$=5μm, $d$=50nm) with the Pt particle (diameter of $d$=50nm) mass loading. Location of the Pt particle is varied from $x$=0 to $x$=1 during calculation.

## S3. Effective Mass and Multimode Resonance Frequencies of CNFs

Based on the mode shapes of the cantilever with the pinned-free boundary conditions, we calculate the effective masses for their flexural resonance motions. The normalized mode shapes can be determined by

$$u_n\left(x\right)=\frac{Z_n(x)}{Z_n(1)}, \tag{S2}$$

where, $Z_n(1)$ is the displacement at the free end cantilever where the displacement is maximum. The effective mass can be determined as

$$M_{\mathrm{eff,CNF},n}=M\int_0^1 u_n\left(x\right)^2\,dx\,. \tag{S3}$$

Here $M$ is the mass of the cantilever. By putting $\beta_n$ into Eqs. S1−S3, we calculate the effective mass of the 1−3 resonance modes to be $M_{\mathrm{eff,CNF},1}$=0.2498, $M_{\mathrm{eff,CNF},2}$=0.2498, and $M_{\mathrm{eff,CNF},3}$=0.2501.

Based on the calculated effective mass, we explore an analytical equation for estimating multimode resonance frequencies of the CNF resonators. The multimode resonance frequencies of the cantilever are determined by

$$f_n=\frac{(\beta_n)^2}{2\pi L^2}\sqrt{\frac{E_{\mathrm{Y}}I}{\rho A}} \tag{S4}$$

where $L$ is the length of the cantilever, $E_{\mathrm{Y}}$ is the Young's modulus, $I=\pi d^4/64$ is the moment of inertia, $\rho$ is the density, $A=\pi d^4/4$ is the cross-section area, and $d$ is the diameter of the cantilever. In our CNF resonator, we cannot use Eq. S4 for calculating resonance frequency since there is a

Nickel (Ni) catalyst on the tip of the CNF. Instead, we modify Eq. S4 to the cantilever with a proof mass on its tip using $f=1/2\pi\times(k_{\mathrm{eff}}/(M_{\mathrm{eff,CNF}}+M_{\mathrm{eff,Ni}}))^{1/2}$, where $M_{\mathrm{eff,Ni}}$ is the effective mass of Ni catalyst. The Ni catalyst is the tip of CNF resonators where the CNF has maximum displacement, thus the effective mass of Ni catalyst is same as its mass ($M_{\mathrm{eff,Ni}}=M_{\mathrm{Ni}}$). Eq. S4 can be modified to

$$f_n=\left(\frac{\beta_n}{\beta_1}\right)^2\left(\frac{CE_{\mathrm{Y}}I}{L^3\left(M_{\mathrm{eff,CNF,n}}+M_{\mathrm{eff,Ni}}\right)}\right)^{1/2}, \tag{S5}$$

where $C$ is 1.5. If the shape of the Ni catalyst is assume to be sphere, we can rewrite Eq. S5 to

$$f_n=\left(\frac{\beta_n}{\beta_1}\right)^2\left(\frac{CE_{\mathrm{Y}}\frac{\pi d^4}{64}}{L^3\left(0.25\pi\left(\frac{d}{2}\right)^2\rho_{\mathrm{CNF}}L+\rho_{\mathrm{Ni}}\pi\frac{4}{3}\left(\frac{d}{2}\right)^3\right)}\right)^{1/2}, \tag{S6}$$

where $\rho_{\mathrm{CNF}}$ is the density of the CNF, $\rho_{\mathrm{Ni}}$ is the density of the Ni catalyst. Based on Eq. S6, we calculate frequency scaling of the CNF cantilever with respect to its diameter (see Fig. S3(a)). We also have examined clamped-free boundary conditions. In the clamped-free conditions, the CNF resonator shown in Figs. 3(c-d) in main text exhibits $E_{\mathrm{Y}}\approx600$GPa which disagrees with the expected Young's modulus of the CNF with the its graphene angle. Instead, we find $E_{\mathrm{Y}}=32$GPa using Eq. S6, which agrees with previously reported results.[1] For calculation, we use $E_{\mathrm{Y}}=32$GPa, and $L=5\mu$m. Also by replacing diameter to cross-sectional area ($A$), $d=2(A/\pi)^{1/2}$, frequency scaling over cross sectional area of the CNF can be obtained (see Fig. S3(b)). The results reveal that larger diameter and cross sectional area of the CNF yield higher resonance frequency.

Eq. S5 also demonstrates that compared with the resonance mode spacing in the conventional clamped-free cantilever ($f_2/f_1$=6.26, $f_3/f_2$=2.80), those in the pinned-free structure ($f_2/f_1$=3.24, $f_3/f_2$=2.09) has richer higher-order modes within narrower frequency bands. This enhanced number of the higher-order modes is particularly suitable for sensing applications, since they have been pursued for multimode sensing of nanoparticles and molecules for achieving precise yet enhanced mass sensitivity.[2,3]

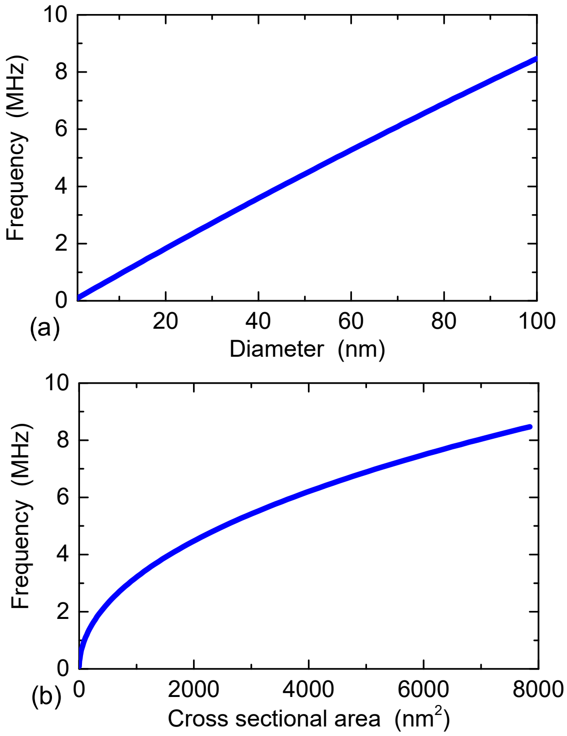

**Figure S3**. Frequency scaling of a CNF cantilever ($L$=5μm) via diameter and cross-sectional area engineering.

## S4. Frequency Scaling of CNFs in Tapered Geometry

Here, we investigate effects of a tapered geometry on the resonance characteristics. Figure S4 shows simulated frequency scaling of the CNF resonator (*L*=5μm, and *d*=50nm) using finite element method (FEM). To make the tapered geometry, we varies the diameter at the tip of the CNF *a*=5−50nm (see Fig. S4(a)) and explore resonance frequencies of the 1-3 modes. The results show that resonance frequencies of 2nd and 3rd modes are decreased as *a*/*d* becomes smaller, while that of the 1st mode is less sensitive to the tapered geometry, leading to smaller frequency spacing between each mode. Also, these findings are consistent with our measured results of reduced mode spacing as shown in the main text.

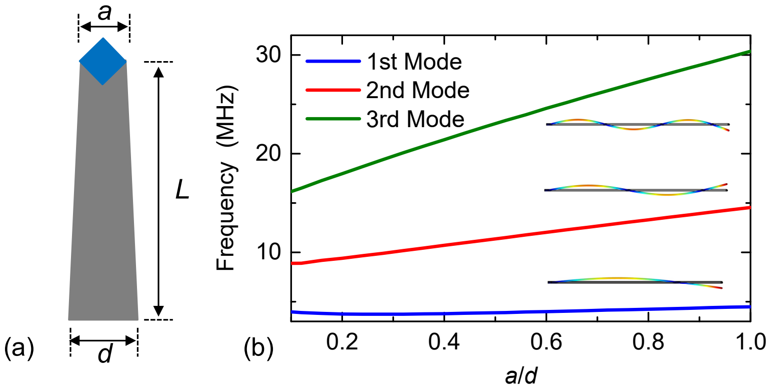

**Figure S4**. Frequency scaling of a CNF resonator (*L*=5μm and *d*=50nm) with tapered geometry. Diameter at the tip of the CNF, *a* is changed from 5nm to 50nm during simulation.

## S5. Localized Mass Loading on CNFs in Different Location

In this section, we investigate effects of localized mass loading on the CNF cantilever. Similar to our experiment that localized platinum (Pt) particle deposition on the CNF resonators in the

SEM, we assume a sphere Pt particle is located on the surface of the CNF cantilever. As we discussed in the previous section, the effective mass of the Pi particle depends on its location and corresponding displacement of the CNF resonator, thus it can be calculated by

$$M_{\mathrm{eff,Pt},n} = M_{\mathrm{Pt}} \left( \frac{Z_{\mathrm{Pt},n}(x)}{Z(1)} \right)^2 , \tag{S7}$$

where, $M_{\mathrm{Pt}}$ is the mass of the Pt particle, and $Z_{\mathrm{Pt},n}(x)$ is displacement of the CNF cantilever where the Pt particle is located. By adding Eq. S7 to Eq. S5, the resonance frequency of the Pt particle loaded CNF cantilever is

$$f_n = \left( \frac{\beta_n}{\beta_1} \right)^2 \left( \frac{C_0 E_{\mathrm{Y}} I}{L^3 \left( M_{\mathrm{eff,CNF,n}} + M_{\mathrm{eff,Pt},n} + M_{\mathrm{eff,Ni}} \right)} \right)^{1/2} . \tag{S8}$$

For calculation, we assume that Pt particle is located on the CNF resonator with $L$=5μm and $d$=50nm. Then we calculate the resonance frequency by changing the location of the Pt particle from the root to the tip of the CNF. Figures S2(d-f) show the calculated resonance frequencies with the Pt particle mass loading, showing the frequency shifts strongly depend on the location of the Pt particle. Importantly, when the particle is located on the nodal point of the resonance mode where the displacement is minimum, resonance frequency is almost invariant. To address this challenge and predict accurate mass loading effects for achieving reliable resonant mass sensors, multimode mass sensing has been pursued.[1,2] Although the location and the mass of the mass loading on the resonator are unknown, both unknown values can be obtained by measuring multimode frequency shifts: two unknown values can be determined by solving two uncorrelated questions. Employing more resonance modes might further improve accuracy and reliability of mass sensing.

Unlike conventional clamped-free cantilevers, our CNF resonators provide richer resonance modes in narrower frequency range (See Fig. S4) thanks to the unique pinned-free boundary conditions and the tapered geometry. Certainly, these unique properties are great advantages over semiconductor nanowire and carbon nanotube (CNT) resonators, exhibiting the promise of CNF resonators for mass sensing application.

We explore linearity of frequency shift due to mass loading. Using Eq. 8, we vary mass of $M_{\mathrm{Pt}}$ from 0 to 10fg and calculate frequency of the first mode of the CNF ($L$=5μm, $d$=50nm, and $E_{\mathrm{Y}}$=32GPa). We assume the mass is uniformly distributed on the resonator thus $M_{\mathrm{eff,Pt},1} \approx 0.25 M_{\mathrm{Pt}}$. As shown in Fig. S5, frequency shift is quite linear below 10fg mass loading if resonance characteristics including effective stiffness and mode shape are unaffected by mass loading due to $M_{\mathrm{eff,Pt},n} << M_{\mathrm{eff,CNF},n}$.

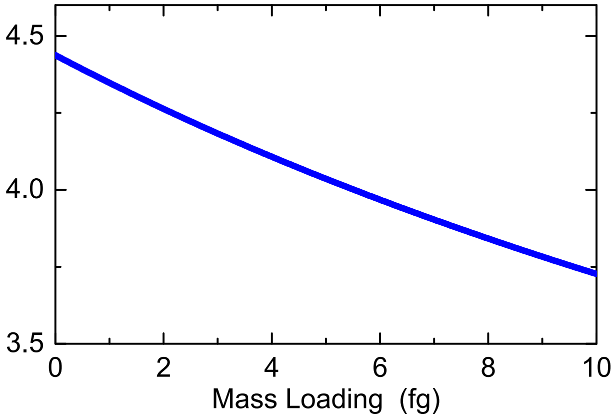

**Figure S5**. Frequency shift of a CNF resonator ($L$=5μm and $d$=50nm) with varying amount of mass loading.

## S6. Photothermal Excitation

The mechanical motion of the resonators can be expressed by

$$\ddot{z}+\frac{\omega_0}{Q}\dot{z}+\frac{k_{\mathrm{eff}}}{M_{\mathrm{eff}}}z=\frac{F_{\mathrm{ext}}}{M_{\mathrm{eff}}}, \tag{S9}$$

where $z$ is the displacement of the resonator, $\omega_0$ is the angular resonance frequency, $k_{\mathrm{eff}}$ is the effective spring constant, and $F_{\mathrm{ext}}$ is the external driving force. When we irradiate laser onto the device, the substrate and the CNF resonator absorb part of the laser power, resulting in temperature elevation. It generates thermal expansion and thus a photothermal force[4]

$$F_{ext}=\beta\left(T_{405}+T_{633}\right). \tag{S10}$$

Here, $\beta$ is the coefficient that converts the device temperature to thermal force. $T_{633}$ and $T_{405}$ are the respective temperature increase due to a 633nm CW laser and a 405nm modulated laser irradiation. The photothermal heating due to the 405nm modulated laser (which irradiates on the substrate) can be expressed as:

$$T_{405}\left(t\right)=a_1\eta c_1 P_{405}\left(1+\gamma\cos\left(\omega t\right)\right), \tag{S11}$$

where $a_1$ is absorbance from the incident 405nm laser to the substrate, $\eta$ is the non-radiative recombination rate, $c_1$ is the constant determined by the device structure (such as geometry, material, laser position relative to the device, *etc.*), $P_{405}$ is the laser power, $\gamma$ is the modulation depth controlled by voltage signal from a network analyzer, $\omega$ is the modulation angular frequency of the 405nm laser. Here, the modulation depth is controlled by output voltage of the network analyzer ($\gamma$=0 for 0mV and 1 for 200mV). When $\omega=\omega_0$ photothermal force can excite resonance motion from thermomechanical motion to driven resonance. In our measurement, with sufficient driving force, the resonance motion of the CNF resonators is excited to ~1.4nm.

## S7. SEM Characterization for Observing Growth Angle of the CNF

In this section, we demonstrate optimized SEM imaging conditions for observing angle between the graphene layers and the central axis of the CNF. Since it consists of the many thin graphene layers, transmission electron microscopy (TEM) is mainly used for investigating its structure. However, TEM characterization requires very careful sample preparation and long measurement time. Here we have developed the optimized SEM imaging conditions for fast characterization of the graphene angle in the CNF. Although conventional SEM imaging such as backscattering electron (BSE) and secondary electron (SE) with Everhart-Thornley detector (ETD) and through the lens detector (TLD) cannot resolve the angle (see Fig. S6(b-d)), imaging with immersion lens and TLD can readily visualize some of the angle (Fig. S6(a)). From this image, we also notice that the graphene angle is mostly uniform from the tip to near the bottom, except the root of the CNF.

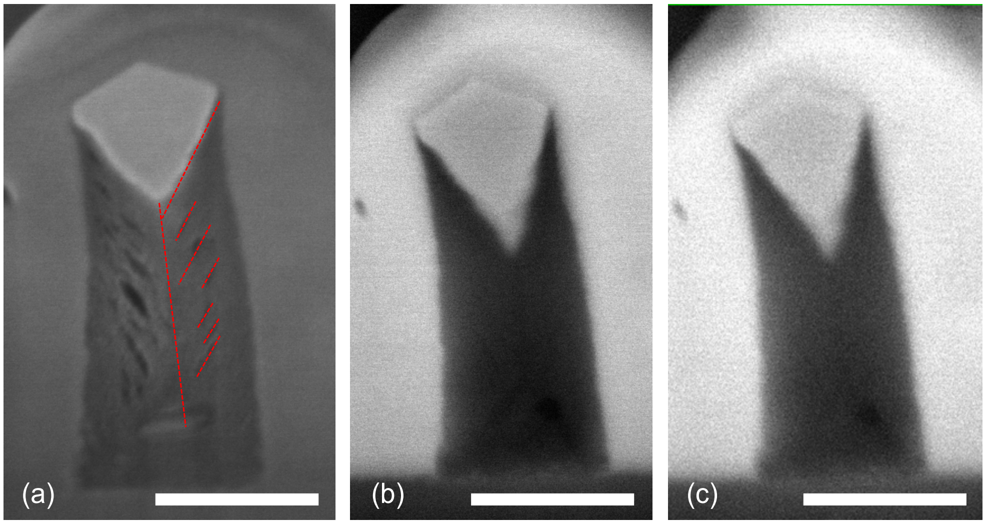

**Figure S6**. Cross-sectional SEM images of the CNF. Images are taken using conditions of (a) 2kV, immersion lens, and TLD; (b) 5kV, BSE, and TLD; (c) 5kV, SE, and ETD. Red dot lines are guidelines for the graphene angle. Scale bars are 300nm.

## S8. Mass Sensitivity in NEMS Resonators

Here, we analyze mass sensitivity of NEMS resonators.[5] When the mass sensitivity, $\delta m$, is in the regime of $\delta m << M_{\text{eff}}$, and $Q$ and effective spring constant $k_{\text{eff}}$ is assumed to be insensitive to mass loading, mass sensitivity is determined by

$$\delta m \approx |\Re|^{-1} \delta\omega_0 = \frac{2M_{\text{eff}}}{\omega_0}\delta\omega_0 , \tag{S12}$$

where $\Re$ is mass responsivity, $|\Re| = \omega/2M_{\text{eff}}$, and $\delta\omega_0$ is noise floor for frequency measurement (*i.e.*, frequency instability). $\delta\omega_0$ can be obtained by integrating the spectrum density of frequency fluctuation,

$$\delta\omega_0 \approx \left[\int_{\omega_0-\pi\Delta f}^{\omega_0+\pi\Delta f} S_\omega(\omega)\,d\omega\right]^{1/2} , \tag{S13}$$

where, $\Delta f$ is the measurement bandwidth. With an employed transducer (*i.e.*, displacement readout system), the spectrum density of frequency fluctuation can be converted to the voltage domain spectrum density, $S_\omega(\omega) = S_V(\omega)/(\partial V/\partial\omega)^2$, where $\partial V/\partial\omega$ is the frequency to voltage conversion rate near the resonance frequency. By assuming $\partial V/\partial\omega$ is linear, it can be approximated to $\partial V/\partial\omega \approx V_{\max}/\Delta\omega = V_{\max}Q/\omega_0$. Based on these relations, frequency noise floor is then

$$\delta\omega_0 \approx \frac{\omega_0}{Q}\frac{\left(S_V\left(\omega\right)2\pi\Delta f\right)^{1/2}}{V_{\max}}. \tag{S14}$$

Here, the ratio of maximum signal to noise floor, $V_{\max}\big/\left(S_V\left(\omega\right)2\pi\Delta f\right)^{1/2}$ is the voltage domain dynamic range (DR) (*i.e.,* linear operation regime) at the resonance due to our assume that $\partial V/\partial\omega$ is linear, thus Eq. S14 is then

$$\delta\omega_0 \approx \frac{\omega_0}{Q}10^{-(\mathrm{DR}/20)}. \tag{S15}$$

Accordingly, by substituting Eq. S15 to Eq. S12, mass sensitivity is determined by

$$\delta m \approx \frac{2M_{\mathrm{eff}}}{Q}10^{(-\mathrm{DR}/20)}. \tag{S16}$$

**Reference**

---

[1] F. A. Ghavanini, H. Jackman, P. Lundgren, K. Svensson, P. Enoksson, *J. Appl. Phys.*, 2013, **113**, 194308.

[2] S. Dohn, R. Sandberg, W. Svendsen, A. Boisen, *Appl. Phys. Lett.*, 2005, **86**, 233501.

[3] M. S. Hanay, S. Kelber, A. K. Naik, D. Chi, S. Hentz, E. C. Bullard, E. Colinet,L. Duraffourg, M. L. Roukes, *Nature Nanotechnol.*, 2012, **7**, 602-608.

[4] B. Ilic, S. Krylov, H. G. Craighead, *J. Appl. Phys.*, 2010, **107**, 034311.

[5] K. L. Ekinci, X. M. H. Huang, M. L. Roukes, *Appl. Phys. Lett.*, 2004, **84**, 4469-4471.